

Biosensors | Hot Paper |

 **Fabrication of Highly Stable Glyco-Gold Nanoparticles and Development of a Glyco-Gold Nanoparticle-Based Oriented Immobilized Antibody Microarray for Lectin (GOAL) Assay**Li-De Huang, Avijit K. Adak, Ching-Ching Yu, Wei-Chen Hsiao, Hong-Jyune Lin, Mu-Lin Chen, and Chun-Cheng Lin^{*[a]}

Abstract: The design of high-affinity lectin ligands is critical for enhancing the inherently weak binding affinities of monomeric carbohydrates to their binding proteins. Glyco-gold nanoparticles (glyco-AuNPs) are promising multivalent glycan displays that can confer significantly improved functional affinity of glyco-AuNPs to proteins. Here, AuNPs are functionalized with several different carbohydrates to profile lectin affinities. We demonstrate that AuNPs functionalized with mixed thiolated ligands comprising glycan (70 mol%) and an amphiphilic linker (30 mol%) provide long-term stability in solutions containing high concentrations of salts and proteins, with no evidence of nonspecific protein adsorption. These highly stable glyco-AuNPs enable the detection of model plant lectins such as Concanavalin A, wheat

germ agglutinin, and *Ricinus communis* Agglutinin 120, at subnanomolar and low picomolar levels through UV/Vis spectrophotometry and dynamic light scattering, respectively. Moreover, we develop in situ glyco-AuNPs-based agglutination on an oriented immobilized antibody microarray, which permits highly sensitive lectin sensing with the naked eye. In addition, this microarray is capable of detecting lectins presented individually, in other environmental settings, or in a mixture of samples. These results indicate that glyco-nanoparticles represent a versatile and highly sensitive method for detecting and probing the binding of glycan to proteins, with significant implications for the construction of a variety of platforms for the development of glyconanoparticle-based biosensors.

Introduction

The adhesive power of low-affinity carbohydrate ligands is amplified by multivalency, a common feature in protein–ligand binding and cell–cell adhesion events.^[1] Lectins, which are abundant in nature, are carbohydrate-binding proteins that are neither antibodies nor enzymes.^[2] In nature, most of these glycan-binding proteins exist as oligomers with several carbohydrate-binding sites. Carbohydrate–protein interactions play an essential role in a variety of pathological and physiological cellular functions such as cell–cell and cell–matrix interactions, inflammation, development, fertility, and cancer metastasis.^[2] The interactions between lectins and host cell-surface carbohydrate epitopes also represent the vital first step in the cycle of host infection by several microbes including bacteria, viruses, fungi, parasites, and protein toxins.^[2,3] For example, proteins involved in infectious pathogenesis, such as the human influ-

enza virus hemagglutinins,^[4] cholera toxins,^[5] and dendritic cell (DC)-specific intracellular adhesion molecule-3-grabbing non-integrins (DC-SIGN) to human immunodeficiency virus (HIV),^[6] are often mediated through binding to terminal glycans on cell-surface glycoproteins. For the prevention of infection, blocking of the glycan-binding proteins or lectins may be beneficial for therapeutic intervention of various disease states. The development of a biosensing platform for the study of these biological interactions at the molecular level would facilitate the elucidation of these biologically significant carbohydrate–ligand interactions.^[7,8]

Accordingly, various multivalent glycoconjugates decorated on a variety of scaffolds, including peptides, dendrimers, synthetic polymers, and proteins, have been designed to control the valency and spatial display of the ligands.^[1] Biomolecule-functionalized nanomaterials are emerging diagnostic tools with unique biological applications in a wide variety of areas.^[9] Of particular interest are the unique optical and electronic properties of gold nanoparticles (AuNPs), which have been used as biosensors in nanomedicine, biomedical imaging, and other biodiagnostic applications.^[10] Glyco-AuNPs, that is, AuNPs decorated with a monolayer of thiolated carbohydrate ligands, can function as excellent nanosized scaffolds similar to the glycocalyx-like structure covering the cell surface.^[11] In addition, these nanomaterials offer several advantages compared with current protein scaffolds, such as greater synthetic control,

[a] Dr. L.-D. Huang,[†] Dr. A. K. Adak,[†] Dr. C.-C. Yu, W.-C. Hsiao, H.-J. Lin, Dr. M.-L. Chen, Prof. Dr. C.-C. Lin
Department of Chemistry
National Tsing Hua University
Hsinchu-300 (Taiwan)
E-mail: cclin66@mx.nthu.edu.tw

[[†]] These authors contributed equally to this work.

 Supporting information for this article is available on the WWW under <http://dx.doi.org/10.1002/chem.201405747>.

a high degree of solubility and stability in buffered aqueous solutions, high-density ligands, and high flexibility.^[12,13] The outer carbohydrate residues located on the surface of glyco-AuNPs could function as multiple antennae, thereby greatly enhancing their ability to detect glycan-mediated interactions *in vitro*.^[14]

Russell and co-workers reported on the use of mannose (Man)-functionalized AuNPs to examine the binding specificity of a well-known plant lectin, Concanavalin A (Con A), by UV/Vis spectrophotometry.^[15] The carbohydrate ligand density on the surface of AuNPs may affect particle aggregation and the overall detection sensitivity. Kataoka and co-workers determined that PEGylated lactose (Lac)-modified AuNPs with 65% surface coverage produced optimal RCA₁₂₀-induced AuNP aggregation.^[16] Although Lac-functionalized PEGylated AuNPs exhibit high dispersion stability in aqueous buffer solutions, these AuNPs are susceptible to the nonspecific adsorption of proteins.^[16] In addition, the type of saccharide presented on the AuNPs and the spacer lengths affect the aggregation of the AuNPs and the detection sensitivity for RCA₁₂₀ significantly.^[17]

Notably, these AuNPs enabled the study of carbohydrate-mediated lectin interactions; however, the investigation was limited to only one type of carbohydrate and one type of lectin. To analyze the carbohydrate–protein interactions quantitatively, various glyconanoparticle systems bearing different carbohydrate epitopes have been described for the investigation of specific binding interactions through several methods.^[18] These methods include surface plasmon resonance (SPR),^[19] quartz crystal microbalance (QCM) techniques,^[20] isothermal titration calorimetry (ITC),^[21] magnetic resonance imaging (MRI),^[22] fluorescence measurements,^[23] and dynamic light scattering (DLS).^[24]

We previously reported that glyco-AuNPs can be used for labeling specific proteins on the cell surface through carbohydrate–receptor interactions.^[13] The AuNPs decorated with Man residues were used to visualize the FimH adhesions on type I pili of *E. coli* by transmission electron microscopy (TEM). Glyco-AuNPs exhibit a strong glycoside cluster effect for presenting carbohydrate ligands that enhance the binding affinity of the carbohydrate to lectin and are potent anti-adhesives for the prevention of bacterial pathogen invasion.^[11,18] In this context, we made quantitative measurements of the binding affinities between the model lectin Con A and various AuNPs carrying multiple copies of Man residues using SPR.^[19] Moreover, we determined that globotriose (Gb3 or blood group antigen, P^k)-coated AuNPs with different particle sizes containing 60 to 1970 sugars on the surface are inhibitors of the B subunit of Shiga-like toxin (Stt-1).^[25] SPR analysis revealed that the relative potencies of each sugar ranged from approximately 1300 for a 4 nm particle with a shorter linker to approximately 228 000 for a 20 nm particle with a longer linker. Thus, glyco-AuNP aggregation could be tuned for use as a newer screening method for monitoring the bond-forming activities of enzymes. For example, we recently demonstrated a high-throughput AuNP-based colorimetric assay for the analysis of the specific bond formation activity of a model enzyme, α -2,8-polysialyltransferase, which catalyzes the biosynthesis of α -2,8-linked polysialic acid.^[26]

Here, we prepared different glyco-AuNPs and demonstrated that glyco-AuNPs can detect cognate lectins at a low picomolar level. We determined that glyco-AuNPs protected with an additional monolayer of an amphiphilic linker are stable under high physiological salt concentrations and are resistant to non-specific protein adherence in solution and on solid supports such as a microarray. Moreover, we present glyconanoparticle-based biosensing with the naked eye of lectins bound to an oriented immobilized-antibody microarray surface (Figure 1).

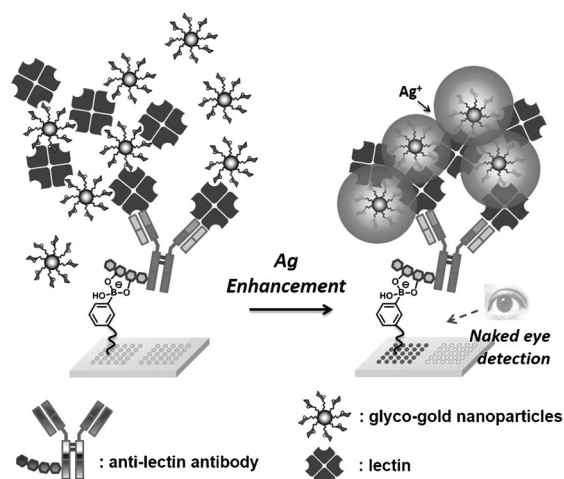


Figure 1. Illustration of a glyconanoparticle-based oriented antibody microarray for lectin sensing (GOAL) assay. The GOAL assay permits direct measurement of carbohydrate–lectin interactions by naked-eye visualization of the surface-bound protein utilizing glyco-AuNPs on glass slides after silver enhancement.

Finally, we demonstrate the feasibility of a functional Ab microarray platform for the simultaneous detection of lectins in samples containing a mixture of analytes. As outlined in Figure 1, when antibodies are immobilized, surface-functionalized boronic acids (BAs) form, in an oriented manner, cyclic boronate diesters with the diol groups of the glycans in the non-antigenic Fc region. This method essentially prevents the antibodies from binding to the solid surface through their antigen-binding Fab domains, which may facilitate accessibility to an incoming antigen. The detection of the bound antigen was visualized by *in situ* agglutination using high-affinity glyco-AuNPs following silver enhancement. Because boronate-mediated immobilization surpassed prior antibody modifications, this assay may provide significantly improved antigen-binding ability and sensitivity compared with methods employing random covalent coupling.

Results and Discussion

Synthesis of thiolated glycans 1–4 and 6–11

Thiolated lactose derivatives (**1**^[27] and **2**^[28]) equipped with a shorter linker or a short alkane-thiolate-terminated lactoside **3** (Figure 2) were synthesized as described previously or in the Supporting Information. To impart flexibility and solubility to

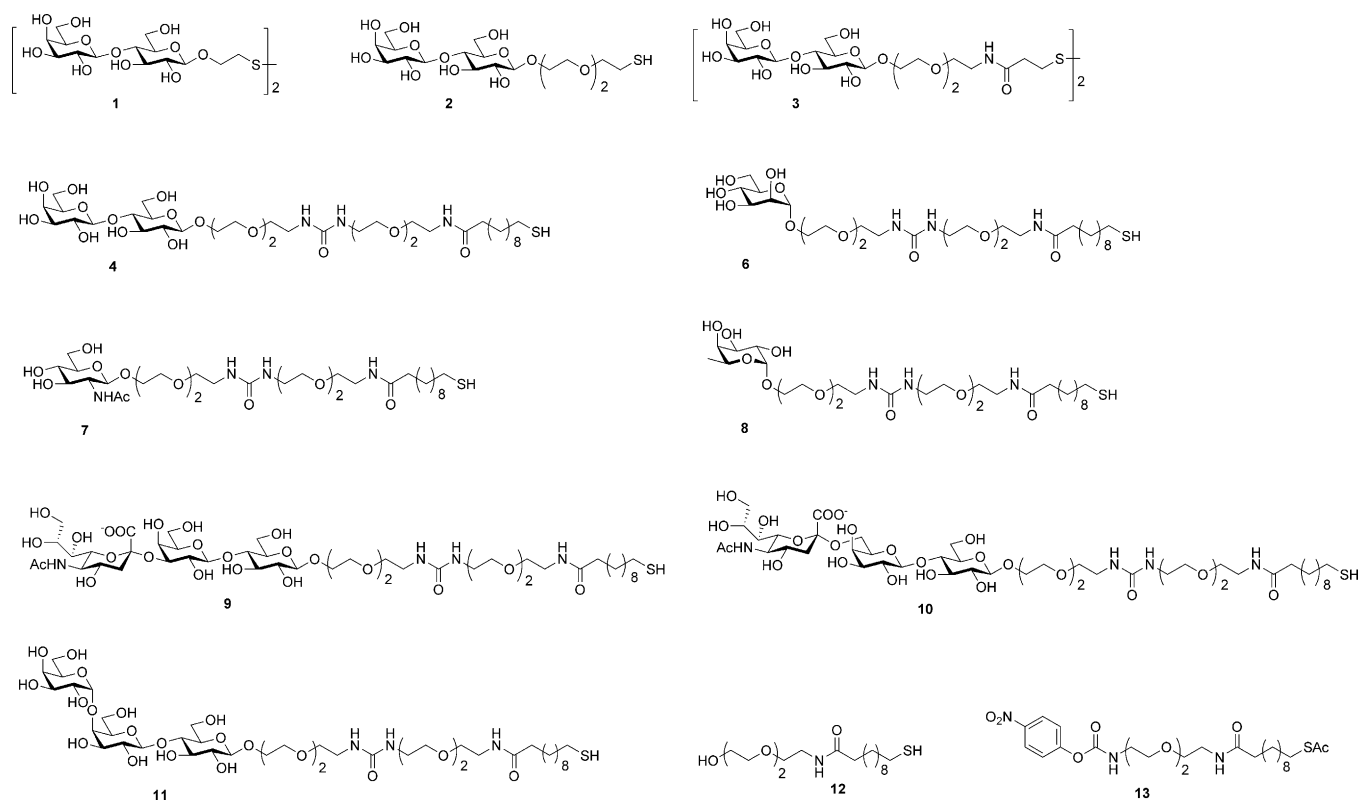


Figure 2. Structures of thiolated glycans (1–4 and 6–11) and a short tri(ethylene glycol) terminated alkanethiol (12) used for the synthesis of glyco-AuNPs.

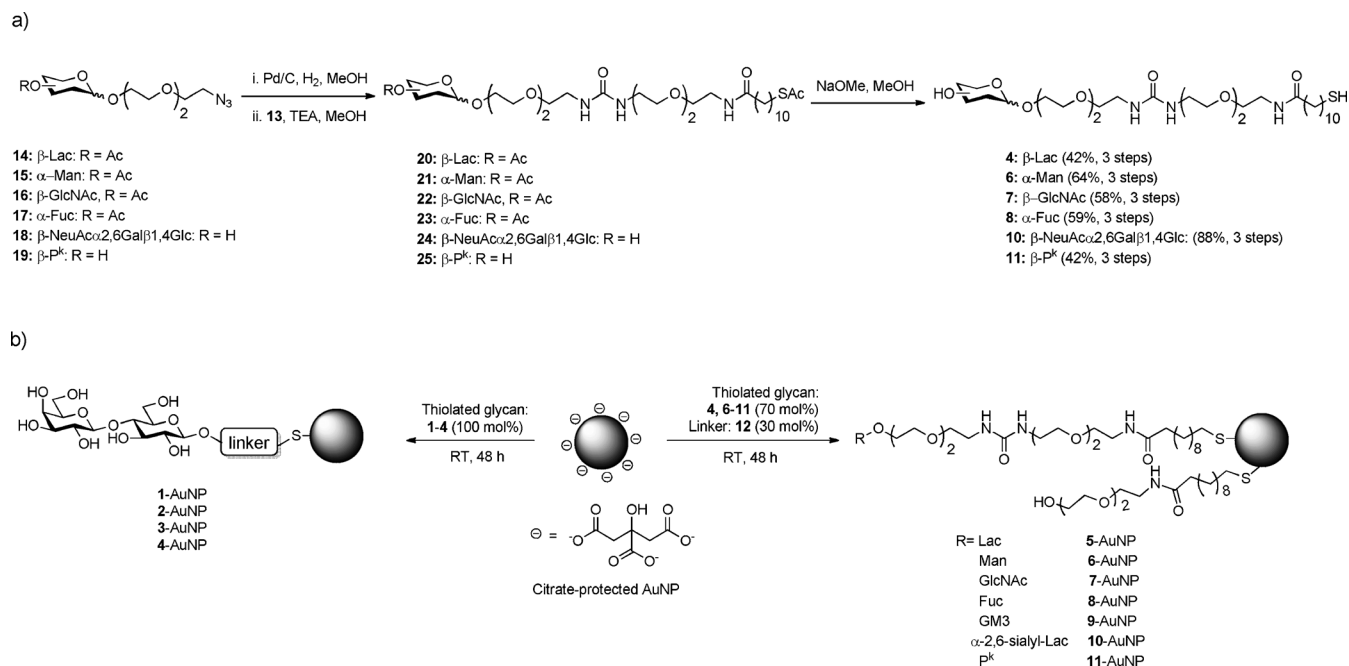
the glyco-AuNPs, we incorporated an amphiphilic mixed aliphatic/ethylene glycol spacer **13** into the neoglycoconjugates.

The *p*-nitrophenyl carbamate-protected neoglycoconjugates could be conjugated easily to the amino-functionalized saccharides through a urea linkage. Compound **4** was synthesized through a procedure developed in our laboratory,^[26] and the versatility of the urea linkage formation was extended to other glycan structures (**15–19**; Scheme 1 a). Briefly, catalytic hydrogenation of the azides (**14–19**) generated the amines, which, without further purification, were subjected to reaction with **13** (structure shown in Figure 2) to give the corresponding glycans as thioacetates. Finally, deacetylation under either Zemplén conditions or aqueous NaOH afforded thiolated glycan derivatives (**4**, **6–8**, **10**, and **11**) suitable for anchoring on AuNPs in good yields. This approach provides an easy-to-handle and efficient technique for installing thiols at the reducing ends of diverse glycans (Figure 2). In addition, we prepared a tri(ethylene glycol)-terminated alkanethiol (**12**; see the Supporting Information for details of the synthesis) and mixed it with a thiolated glycan to fabricate water-soluble glyco-AuNPs with minimal nonspecific binding to proteins. Furthermore, the AuNPs with a self-assembled monolayer (SAM) of poly(ethylene glycol) exhibited minimum nonspecific adsorption of proteins.^[29]

Preparation of glyco-AuNPs

All of the glyco-AuNPs were synthesized and characterized following established procedures.^[25,26] Briefly, the chemisorbed

citrate molecules on the AuNP surface were replaced with thiolated carbohydrates through a ligand-exchange reaction and Au–S bond formation to give glyconanoparticles (Scheme 1 b). The ligand-exchange reaction enabled not only 100% decoration of AuNPs with a single thiolated glycan but also the assembly of two different thiolated ligands on the AuNPs with varying glycan ratios. Glyco-AuNPs (**1–AuNP** to **4–AuNP**) anchored with thiolated lactose derivatives (**1–4**) were prepared to investigate the effect of spacer length on the stability of the resulting AuNPs in solutions of high ionic strength (100 mM NaCl). The glycan surface densities on the glyco-AuNPs (**5–AuNP** to **11–AuNP**) were varied by using solutions consisting of a mixture of glycans **4–11** (70 mol%) and an amphiphilic linker **12** (30 mol%). The glyco-AuNPs (**1–AuNP** to **11–AuNP**) were purified by repetitive centrifugation and resuspension in either 10 mM Tris buffer (pH 7.4) or 10 mM phosphate-buffered saline (PBS; pH 7.4). The glyco-AuNPs were fairly dispersed in aqueous buffer solutions and displayed a redshifted surface plasmon resonance (SPR) peak at 525 nm, which was associated with the attachment of thiolated ligands, indicating no self-aggregation upon surface modification with saccharide (see the Supporting Information, Figure S2). This small (5 nm) peak shift is attributable to the formation of a dense organic layer by the replacement of citrates on the AuNP surface, which correlates significantly with the dielectric constant of the medium surrounding the nanoparticles.^[30]



Scheme 1. Synthesis of a) thiolated glycans (4, 6–8, 10, and 11), and b) glyco-AuNPs (1–AuNP to 11–AuNP). For detailed structures of the thiolated glycans used for glyco-AuNP synthesis, see Figure 2.

Effect of spacer length and carbohydrate ligand density of glyco-AuNPs on their stability in high salt concentrations and resistance to nonspecific protein adsorption

AuNPs are prone to aggregation in solutions of high ionic strength or under physiological conditions.^[31] Therefore, for biological use, AuNPs must exhibit long-term stability without nonspecific aggregation in solutions containing high concentrations of proteins and salts. For the determination of the nonspecific agglomeration of AuNPs, the colloidal dispersion stability of glyco-AuNPs (1–AuNP to 5–AuNP) was assessed under physiological conditions (Figure 3 and Figure S3). The short spacers on the AuNPs provide increased colorimetric detection sensitivity but also increase aggregation.^[17] Upon exposure of nanoparticles (1–AuNP to 3–AuNP) to a solution with a high NaCl concentration (12.5–600 mM), immediate aggregation was observed, indicating that these AuNPs are unsuitable for lectin-sensing applications. In contrast, 4–AuNP containing a linker with a lipophilic undecyl unit and a tri(ethylene glycol) chain exhibited very little change in the surface plasmon absorption band under the same conditions (Figure 3a, dotted line), suggesting superior stability to nanoparticles 1–AuNP to 3–AuNP. The slight change in the intensity of the plasmon band may be attributed to imperfect SAM formation on the nanoparticle surface owing to steric hindrance between the Lac head groups.^[32] Thus, to reduce the hindrance to the formation of a perfect SAM on the AuNPs, we incorporated an amphiphilic linker (12) to give 5–AuNP. In the high-salt solutions (NaCl concentration from 12.5 to 600 mM), 5–AuNP remained stable, and no change in the absorption intensity was observed (Figure 3a, solid line). These findings provide useful cues for the construction of highly stable, mixed monolayer

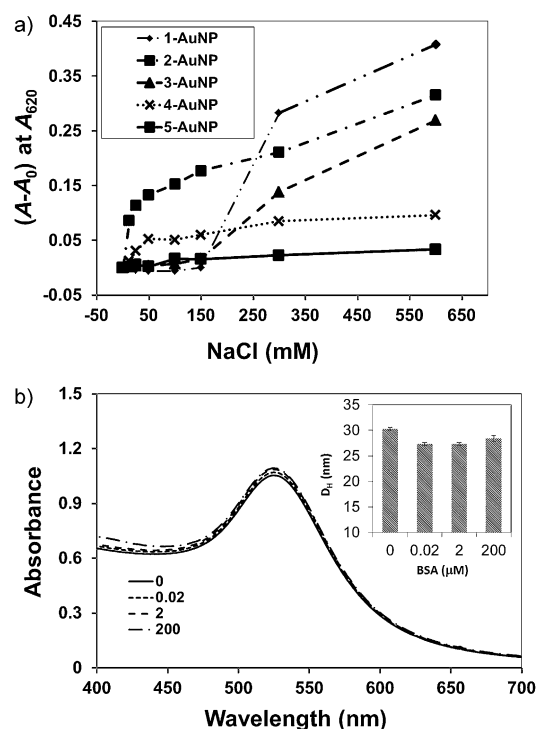


Figure 3. The effects of different aglycone lengths and ionic strengths on the stability of glyco-AuNPs. a) The stability of glyco-AuNPs in various NaCl solutions. Changes in the SPR band intensities [(A–A₀)/A₀], A₀ = initial absorbance, and A = absorbance after 8 h] of different Lac-AuNPs (1–AuNP to 5–AuNP) in the presence of varying concentrations of NaCl at 620 nm after 8 h at room temperature. b) The UV/vis absorption spectra of 5–AuNP treated with BSA at concentrations of 0, 0.02, 2, and 200 μM in PBS after 8 h incubation. The inset shows the corresponding D_p of 5–AuNP in the presence of BSA at each indicated concentration.

protected glyco-AuNPs for bioanalytical assays (see below) similar to that of PEGylated AuNPs.^[16]

In addition to enhancing the colloidal stability of glyco-AuNPs in high physiological salt conditions (NaCl, 150 mM), the presence of **12** led to little or no nonspecific protein adsorption. As shown in Figure 3b, no apparent changes in the surface plasmon absorbance and hydrodynamic diameter (D_H) were observed upon treatment of 5-AuNP with bovine serum albumin (BSA; 0.02 to 200 μ M), indicating that the mixed monolayer renders the AuNPs inert to nonspecific adsorption of proteins in solution. Although 2-AuNP obviated nonspecific binding to BSA (see the Supporting Information, Figure S4), 1-AuNP, which lacks the **12** monolayer, exhibited nonspecific BSA adsorption as indicated by the UV/Vis spectrum and DLS measurements (see the Supporting Information, Figure S5). Nevertheless, the presence of **12** is crucial because it not only imparts steric hindrance to proteins that could be nonspecifically adsorbed on the nanoparticle surface, but also provides a good nanoparticle packing density in aqueous solution.^[33] Furthermore, glyco-AuNPs containing other glycan structures with linker **12**, such as 6-AuNP and 7-AuNP, also exhibited no change in the surface plasmon absorption band; consequently, the nonspecific adsorptions were insignificant (see the Supporting Information, Figure S6). These results indicate that a 30% monolayer of **12** in glyco-AuNPs impedes nonspecific protein attachments, in good agreement with an earlier report that an ethylene glycol monolayer prevents the nonspecific binding of proteins such as BSA to AuNPs.^[34]

Recognition of glyco-AuNPs by lectins

Lectins have been employed widely as a model system for investigating how proteins recognize glycans on a molecular level through selective carbohydrate-protein interactions. The recognition between lectins and glycans essentially occurs through multiple low-affinity interactions. Glyco-AuNPs have potential as ideal scaffolds for presenting multiple carbohydrates, and are similar in size to many biomolecules. For further investigation of the specific binding interactions of lectins and carbohydrates, a representative panel of seven different lectins was selected. Table 1 summarizes the synthetic AuNPs used in this study and the lectin specificity to the corresponding glycan structures present on the synthesized glyco-AuNPs. We describe here a sensitive plate-based colorimetric assay for rapid profiling of the presence of lectins. In this assay, lectins

Table 1. The lectins, their carbohydrate ligands, and the corresponding glyco-AuNP ligands.			
Glyco-AuNP	Lectin	Carbohydrate ligand recognized	[Ref.]
5-AuNP	RCA ₁₂₀	Lac: Gal β 1,4Glc	[35]
6-AuNP	Con A	α -D-Man	[36]
7-AuNP	WGA	β -D-GlcNAc	[37]
8-AuNP	AAL	α -L-Fuc	[38]
9-AuNP	MAL	GM3: NeuAc α 2,3Gal β 1,4Glc	[39]
10-AuNP	SNA	NeuAc α 2,6Gal β 1,4Glc	[40]
11-AuNP	PA-IL	Gb3: Gal α 1,4Gal β 1,4Glc	[41]

induce the aggregation of glyco-AuNPs, which is reflected in the color change of the glyco-AuNP from red to purple or blue, and can be seen easily with the naked eye.

As shown in Figure 4a, lectins specifically recognize and bind to their cognate carbohydrate ligands present on the sur-

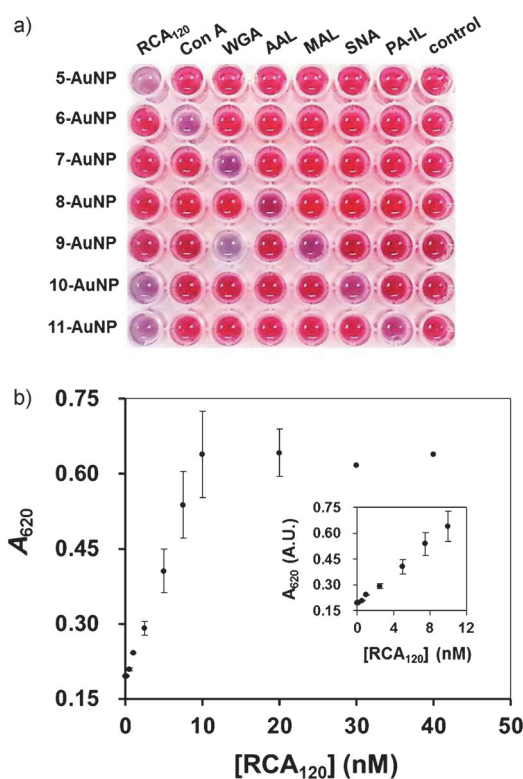


Figure 4. Glyco-AuNP-based colorimetric lectin assay. a) Plate-based colorimetric assay for lectins with different glyco-AuNPs (5-AuNP to 11-AuNP). b) AuNP-based colorimetric detection of RCA₁₂₀. The inset shows the linear range from 0 to 10 nM RCA₁₂₀ concentration, which was used to calculate the limit of detection (LOD) for RCA₁₂₀.

faces of the glyco-AuNPs. Of these plant lectins, Con A, MAL, and SNA displayed good affinities to 6-AuNP, 9-AuNP, and 10-AuNP, respectively. As expected, the fungal lectin AAL, which recognizes the L-fucose residue, exhibited preferential binding to 8-AuNP. The bacterial lectin PA-IL, which recognizes only Gb3 glycans, only interacted with 11-AuNP. Despite possessing a nominal binding specificity for Lac (Gal β 1,4Glc), RCA₁₂₀ also binds nonreducing Gal-modified Lac. The results of the colorimetric assays revealed strong RCA₁₂₀ binding to nonreducing terminal Gal, such as that found in the P^k antigen^[42] (11-AuNP) and NeuAc α 2,6-Gal^[43] (10-AuNP), but not NeuAc α 2,3-Gal, in good agreement with previous reports. Conversely, the GlcNAc-specific lectin WGA exhibited preferential binding to 7-AuNP, as predicted, but also interacted with the NeuAc α 2,3-Gal-terminating structure (9-AuNP), also in accordance with literature data.^[44] Addition of the free carbohydrates Lac (10 mM), Man- α -OMe (100 mM), or GlcNAc (500 mM) in excess to aggregated AuNP solutions containing RCA₁₂₀ and 5-AuNP, Con A and 6-AuNP, or WGA and 7-AuNP, respectively, promoted complete redispersion of the aggregates along with recov-

ery of the original surface plasmon band (data not shown). These results indicate that the aggregation was specifically caused by carbohydrate–lectin interactions. Furthermore, reciprocal experiments between glyco-AuNPs (5–AuNP, 6–AuNP, and 7–AuNP) and lectins such as RCA₁₂₀, Con A, and WGA revealed no nonspecific binding between carbohydrates and lectins. These results clearly indicate the potential for the use of glyco-AuNPs in the detection of target lectins.

Determination of the detection sensitivity of different lectins by UV/Vis spectroscopy and DLS

Next, we investigated the detection sensitivity of the AuNP-based colorimetric bioassay for individual lectins by using UV/Vis spectroscopy (Table 2). The assays were performed by treat-

Table 2. LODs of lectins estimated by different methods using glyco-AuNPs.				
Glyco-AuNP	Lectin	Colorimetric [pM] ^[a]	DLS [pM] ^[b]	GOAL assay ^[c]
5–AuNP	RCA ₁₂₀	300 (7 nM) ^[17]	3 (6.6 nM) ^[24]	1
6–AuNP	Con A	430 (6.2 nM) ^[23]	16 (15 nM) ^[24]	5
7–AuNP	WGA	500 (1.5 nM) ^[45]	12	1

The LOD values were calculated as follows: [a] LOD = signal of the blank + 3*standard deviation (SD). [b] LOD = 3*SD of the blank/slope of the calibration curve. [c] Determined as the lowest concentration that produced a detectable signal after silver enhancement. The corresponding LOD values reported in the literature are shown in parentheses.

ing 5–AuNP (3 nM) with a range of concentrations of RCA₁₂₀ (0, 0.1, 0.5, 1, 2.5, 5, 7.5, 10, 20, 30, and 40 nM), a potential surrogate for the bioterrorism agent ricin. The aggregation of 5–AuNPs was indicated by the color change of the AuNPs from red to blue (see the Supporting Information, Figure S7) and a simultaneous change in the absorption band in the visible region of the electromagnetic spectrum (Figure 4b). As illustrated in Figure 4b, the plot of the change in the SPR band intensity at 620 nm versus various concentrations of RCA₁₂₀ reveals a linear concentration-dependent aggregation from 0 to 10 nM, with a limit of detection (LOD) for RCA₁₂₀ of 300 pM (Table 2), which is 23 times higher than that estimated from optimally presented Gal-coated AuNPs.^[17] The higher detection sensitivity of 5–AuNP may be attributed to its superior stability and optimal presentation of Lac head groups in an ordered monolayer. These nanoparticles enable more efficient intimate contacts with the carbohydrate-binding sites of the lectin.^[11,18] On the basis of this colorimetric bioassay (Table 2), subnanomolar detection sensitivities (or LODs) for Con A (430 pM) and WGA (500 pM) were also achieved using 6–AuNP and 7–AuNP within a linear range from 0.1 to 10 nM and 0.5 to 7.5 nM for Con A and WGA, respectively (see the Supporting Information, Figure S8).

The AuNP-based colorimetric sensing method was also compared with the results obtained using DLS (Table 2). The LOD for RCA₁₂₀ was 3 pM (see the Supporting Information, Fig-

ure S9), which is 2.2×10^3 times more sensitive than a Gal-functionalized silica nanoparticle in a DLS assay.^[24] The LOD for Con A using 6–AuNP was 16 pM, which is approximately 9.7×10^2 times higher than a similar DLS measurement.^[24] The sensitivity for WGA was as low as 12 pM if 7–AuNP was used. Notably, most colorimetric sensors based on nanoparticle aggregation exhibit LODs greater than 1.5 nM,^[18,23,24,45] however, the LODs are improved to low picomolar levels by employing DLS.

Glyconanoparticle-based oriented antibody microarray for lectin sensing (GOAL assay)

We previously developed a covalent and site-specifically immobilized Fc-fused lectin microarray, and demonstrated that the oriented, immobilized lectin retained higher lectin activity compared with random immobilization.^[46] The use of BA as an affinity head group to direct the orientation of the antibody has been extended to immobilize them on solid supports such as magnetic nanoparticles.^[47] Furthermore, we previously used a typical “sandwich” approach for the detection of the B subunit of Slt-I bound to a randomly immobilized antibody microarray surface, achieving a detection sensitivity of around 70 nM.^[25] Therefore, to develop a glyco-AuNP-based immunosensing platform, we hypothesized that an oriented antibody microarray could be constructed using BA-derivative **26**, which would preserve the activity of the immobilized antibody, resulting in an improved detection sensitivity.^[48] Because of its hydrophilic nature, the tri(ethylene glycol) spacer in **26** prevented nonspecific adsorption and minimized detrimental interactions between the attached protein and the solid surface.^[49] A homogeneous interaction of the bound antigen could also be achieved by simultaneous incubation of the high-affinity glyco-AuNPs on the microarray surface. These studies would validate the utility of the multivalent effect for designing a glyconanoparticle-based oriented antibody microarray for lectin sensing (GOAL assay; Figure 1). For implementation of the GOAL assay, the effect of the size of the nanoparticle, which serves as the seed for silver enhancement, on the visualization of in situ agglutination was first investigated (Figure 5). Lectin-induced in situ AuNP agglutination with visual detection is an easy-to-use method that avoids the use of sophisticated instruments for the elucidation of carbohydrate-mediated interactions.

As a demonstration of the feasibility of the GOAL assay, the anti-RAC (A-chain) antibody (10 μM) was fabricated on a **26**-coated surface (50 nM). Following blocking with dextran (100 μM containing 1% BSA), the slide was incubated with a solution of RCA₁₂₀ (20 nM) and 5–AuNP (5 nM) for 8 h at room temperature (Figure 5a). As a control, the anti-RAC antibody (10 μM) was immobilized randomly on a Nexterion H slide by amide bond formation, followed by simultaneous incubation with RCA₁₂₀ and 5–AuNP, as described above (Figure 5b). RCA₁₂₀ is a heterodimeric protein consisting of two A–B subunits and a Lac-binding site on each B subunit.^[35] Therefore, the lectin can act as a crosslinker. Antibodies on the surface captured the A chain(s) of RCA₁₂₀, and the remaining two Lac-binding B chains and RCA₁₂₀ in solution aggregated simultaneously

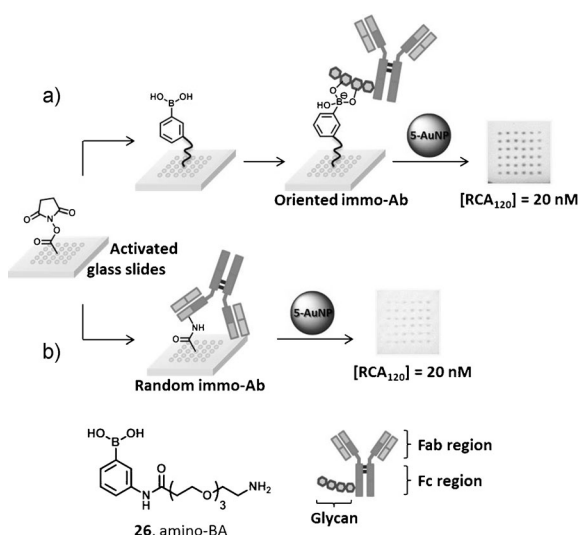


Figure 5. Schematic depiction of the GOAL assay for lectin detection. The capture antibody ($10 \mu\text{M}$) that recognizes lectin, RCA_{120} , was fabricated by a) oriented immobilization through boronate formation using a BA derivative (**26**), and b) random amide bond formation on an NHS-activated glass slide. The presence of the bound antigen was detected by simultaneous incubation with RCA_{120} (20 nM) and a high-affinity glyco-AuNP, 5-AuNP (5 nM), followed by silver enhancement.

with 5-AuNPs. Following a final wash, the array slides were exposed to the silver amplification solution for 14 min to darken the aggregated AuNPs to enable visualization of the spots with the naked eye. As evident from the silver-enhanced image in Figure 5a, the antibody microarray immobilized in an oriented manner produced a homogeneous array definition, whereas the microarrays fabricated by random antibody immobilization furnished a very weak signal after silver enhancement (Figure 5b). The appearance of darker spots in the former method may be because of the increased capture of AuNPs on the slide surface. This increased capture may occur because the surface-conjugated BAs direct the formation of cyclic boronate diesters with the diol groups of glycans at the Fc region of the antibody, thereby leaving the Fab region exposed to the interface for enhanced antigen capture^[50] and leading to a greater number of AuNP seeds available for nucleation. The results strongly suggest that the orientation of antibodies on the microarray is significant for the enhancement of the detection sensitivity.

LODs of different lectins in the GOAL assay

After establishing that orientation is critical for providing improved antibody activity during in situ agglutination, we then used the GOAL assay to estimate the detection sensitivities of different antigens. For further optimization of the detection sensitivity of the GOAL assay, the effects of incubation time (1–8 h) and AuNP concentration (0.5–5 nM) were investigated (see the Supporting Information, Figure S10). For a fixed concentration of RCA_{120} (10 nM), a 5 nM concentration of 5-AuNP and a 2 h incubation time produced an acceptable level of array definition. Therefore, these optimal conditions were used for

further immunosensing experiments for LOD measurements (see below).

For the determination of the LOD of RCA_{120} , the array slide was exposed to $100 \mu\text{L}$ of solutions of different concentrations of RCA_{120} (1–10 nM, final concentration) and 5-AuNP (5 nM) with gentle agitation at 30 rpm for 2 h. As shown in Figure 6a,

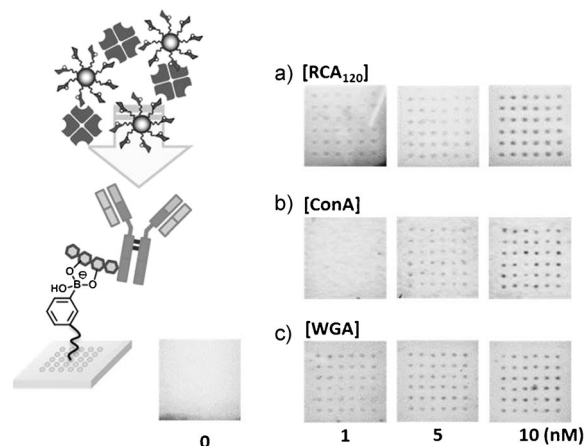


Figure 6. In situ lectin-induced glyco-AuNP agglutination immunoassay for lectin detection. Silver-enhanced images of slides after incubation with a) RCA_{120} (1, 5, and 10 nM) with 5-AuNP; b) Con A (1, 5, and 10 nM) with 6-AuNP; or c) WGA (1, 5, and 10 nM) with 7-AuNP for 2 h. A representative control slide without RCA_{120} and exposed to 5-AuNP is also shown. The immunoassay was performed with lectin solutions in PBS buffer. All images were acquired with a flatbed scanner.

spots were clearly identified at concentrations as low as 1 nM RCA_{120} after silver enhancement. No spots were observed on the control slide without RCA_{120} , demonstrating that neither nonspecific adherence of the AuNPs to the immobilized antibody nor nonspecific silver deposition on the bare glass occurred. Importantly, additional control experiments using glyco-AuNPs (1-AuNP to 3-AuNP) lacking a mixed monolayer revealed nonspecific adsorption on the slide surface or on the antibodies (see the Supporting Information, Figure S11). On the basis of the visible spots formed by specific agglutination and silver precipitation, a detection sensitivity of 1 nM was achieved. This sensitivity is approximately six times greater than that of reported literature methods based on UV/Vis spectroscopy and DLS (see Table 2).^[17,24]

We suggest that the observed sensitivity comes from the control of the orientation of the antibodies on the BA surface, which increases the area available for antigen binding, resulting in stable complexes with a high antigen/antibody ratio. AuNPs can undergo a favorable (homogeneous) interaction with RCA_{120} binding sites in solution owing to the minimal surface steric hindrance, which induces increased AuNP aggregation during in situ agglutination. Notably, the shortest distance between two binding sites in RCA_{120} is approximately 10 nm .^[51] Therefore, the glyco-AuNP 5-AuNP (15 nm core diameter) used in the present study, which has a circumference of around 47 nm , may permit complete insertion of Lac into the binding pocket of RCA_{120} . This insertion leads to the formation of many

layers on the microarray surface similar to the previously described binding of RCA₁₂₀ using AuNPs with 70% Gal coverage.^[17] Upon examination of Con A and WGA, similarly low nanomolar detection sensitivities of 5 nM and 1 nM, respectively, were established (Figure 6b,c and Table 2). Nevertheless, these results demonstrate that selective in situ agglutination of AuNPs on microarrays can be applied widely for the detection of carbohydrate-binding proteins.

Although a low picomolar-level lectin-sensing platform could be realized on the basis of DLS measurements (Table 2), we have determined that this method is not capable of detecting analytes in the context of environmental settings, such as in samples from lake water. The strong background scattering contributes more significantly to the absolute scattering light intensity despite prior passage of the sample through a 0.45 μm filter (see the Supporting Information, Figure S12a). Therefore, the DLS-based assay is unsuitable for samples in such conditions. The SPR band of 5-AuNP in lake water remained unchanged at 525 nm, suggesting that 5-AuNPs are stable and do not aggregate even in the presence of other microparticles (Figure S12b). Notably, our GOAL assay was still able to detect 2.5 nM RCA₁₂₀ under these conditions (Figure S12c). These findings highlight the potential of the GOAL assay for the sensing of analytes under diverse environmental stress conditions.

Simultaneous detection of multiple antigens

As a demonstration of the capability of this newly developed method for multiple lectin detection, the GOAL assay was used to detect multiple lectins in the same sample. Capture Ab spots (12 replicate spots per Ab) were printed in a 2×6 array format on a 26-functionalized glass slide to detect the presence of RCA₁₂₀ (20 nM), Con A (20 nM), and WGA (20 nM) on a single microarray. Figure 7b–e shows the representative silver-enhanced images obtained when these three lectins were presented as a single lectin (Figure 7b–d) or as a mixture of multiple lectins (Figure 7e). Detection was achieved by exposure of each microarray to the following glyco-AuNPs (5 nM), each aimed at one of the target lectins; 5-AuNP, 6-

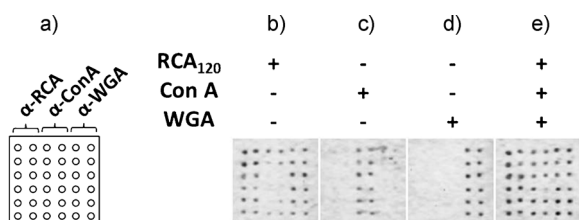


Figure 7. Simultaneous detection of multiple lectins using the GOAL assay. a) A microarray was patterned on each column with twelve replicate capture Ab spots (anti-RAC (A-chain) pAb, anti-Con A pAb, and anti-WGA pAb) corresponding to three lectins as depicted in the schematic. Three samples containing a single lectin (b–d) and one sample containing a mixture of three lectins (e) were incubated for 2 h. The detection of bound lectin (20 nM) was visualized with the corresponding glyco-AuNPs followed by silver enhancement. Representative photographs of the microarray after silver staining for 14 min: b) RCA₁₂₀, c) Con A, d) WGA, and e) three lectins.

AuNP, and 7-AuNP. Silver enhancement was then performed to enlarge and darken the captured nanoparticles.

As shown in Figure 7b–d, each lectin produced distinct spots at appropriate regions where its cognate capture Ab was immobilized on the surface. In addition, Figure 7e clearly indicates the spots resulting from a solution containing all three lectins. Minimal nonspecific binding was observed. The only lectin that exhibited strong cross-reactivity was RCA₁₂₀. When detected as part of a multiantigen immunosensing assay, RCA₁₂₀ recognized and bound both anti-WGA and anti-Con A antibodies (Figure 7b). This cross-reactivity may be caused by glycosylation of the anti-WGA and anti-Con A antibodies by additional NeuAcα2,6Gal- or terminal Gal-containing glycan structures accessible for binding to lectin RCA₁₂₀, which can function as a glycoprotein.

Conclusions

In conclusion, we have developed highly stable, mixed-monolayer-protected glyco-AuNPs and used them as model nanocarriers to study the specific biomolecular recognition between lectins and carbohydrates. These glyco-AuNPs exhibited complete resistance to nonspecific protein adherence in solution and on solid supports. Specific binding interactions for different carbohydrates and lectins, such as RCA₁₂₀ with Lac, Con A with Man, and WGA with GlcNAc, were established on the basis of colorimetric and DLS measurements. The lectin analytes were detected individually by utilizing in situ glyco-AuNPs agglutination-based immunosensing on oriented antibody microarrays with the naked eye. The method is applicable regardless of the lectins and type of saccharides present on the nanoparticles. We have also described the ability of glyco-AuNP-based immunosensing to detect multiple lectins in samples with low nonspecific cross-reactivity. Owing to the ease of detection and the miniature format of this array technology, we anticipate that the glyco-AuNP-based immunosensing strategy is amenable to the production of chips for applications in bioassays and biorecognition.

Experimental Section

General experimental methods

See the Supporting Information for details of general experimental methods.

Syntheses

The syntheses of thiolated lactoside **3**, linker **12**, and amino-terminated tri(ethylene glycol)-linked boronic acid (**26**) are described in the Supporting Information. Azido-terminated tri(ethylene glycol)-linked saccharides **14**,^[52] **15**,^[53] **16**,^[54] **17**,^[55] and linker **13**^[26] were obtained by following literature procedures as described previously. The thiolated α-2,3-sialyllactoside (**9**)^[26] and azido-terminated P^k trisaccharide (**19**)^[56] were obtained from chemoenzymatic methods we described recently. α-2,6-Sialyllactoside derivative **18** was synthesized (see the Supporting Information) in an analogous manner, as reported by us.^[26]

Synthesis of compound 6

Palladium on carbon (Pd/C; 100.0 mg; 10% Pd content) was suspended in a solution of azido α -mannoside **15** (500.0 mg, 0.99 mmol) in MeOH (20 mL) in the presence of AcOH (0.3 mL, 5.24 mmol). The flask was purged with H₂, and a hydrogen balloon was attached. The solution was stirred for 3 h at ambient temperature, and the catalyst was filtered off through a pad of Celite. The Celite bed was washed with MeOH, and the combined filtrates were concentrated under reduced pressure to provide the amine, which was used in the next step without further purification. Triethylamine (1.4 mL, 10.06 mmol) and linker **13** (660 mg, 1.2 mmol) were added to a solution of amine in dichloromethane (30 mL) at -20 °C. The resulting mixture was warmed gradually to room temperature and stirred for another 6 h until TLC indicated complete disappearance of the starting material. The reaction mixture was partitioned into dichloromethane and water. The organic layer was washed successively with saturated NaHCO₃ (aq.), 1 M aqueous HCl, and brine, then dried over MgSO₄, filtered, and concentrated in vacuo. Purification by silica gel column chromatography yielded **21** (613 mg, 0.68 mmol, 69% over two steps). *R*_f = 0.42 (MeOH/DCM = 1:15); [α]_D²⁰ = +21.83 (*c* = 1 in MeOH); ¹H NMR (400 MHz, CDCl₃): δ = 6.22 (br s, 1H, -NH-), 5.17–5.39 (m, 5H, H2, H3, H4, -NH-), 4.86 (d, *J* = 1.6 Hz, 1H, H1), 4.25 (dd, *J* = 5.0, 12.4 Hz, 1H, H6a), 4.03–4.14 (m, 2H, H6b, H5), 3.76–3.84 (m, 1H, -OCH₂-), 3.48–3.73 (m, 17H, -OCH₂-), 3.29–3.46 (m, 6H, -NHCH₂-), 2.82 (t, *J* = 7.4 Hz, 2H, -CH₂S-), 2.29 (s, 3H, -(C=O)CH₃), 2.15 (t, *J* = 7.4 Hz, 2H, -(C=O)CH₂-), 2.13 (s, 3H, -(C=O)CH₃), 2.08 (s, 3H, -(C=O)CH₃), 2.01 (s, 3H, -(C=O)CH₃), 1.95 (s, 3H, -(C=O)CH₃), 1.46–1.66 (m, 4H, -CH₂-), 1.15–1.38 ppm (m, 12H, -CH₂-); ¹³C NMR (100 MHz, CDCl₃): δ = 195.9, 173.5, 170.6, 169.9, 169.5, 158.4, 97.4, 70.6, 70.5, 70.4, 70.2, 70.0, 69.9, 69.7(×2), 69.3, 68.9, 68.1, 7.2, 65.8, 62.2, 39.8(×2), 39.0, 36.4, 30.4, 29.2, 29.2(×2), 29.1, 29.0, 28.9, 28.8, 28.5, 25.5, 20.7, 20.6, 20.5 ppm; HRMS (ESI): *m/z* calcd for C₄₀H₇₀N₃O₁₇S [M+H]⁺: 896.4426; found: 896.4459. The fully protected thiolated mannoside **21** (450 mg, 0.50 mmol) was dissolved in dry MeOH (10 mL), and NaOMe (40.5 mg, 0.75 mmol) was added. The resulting mixture was stirred at room temperature for 1 h and neutralized with Amberlite ion-exchange resin IR 120. After filtration and concentration, flash silica gel column chromatography provided thiolated mannoside derivative **6** (220 mg, 0.32 mmol, 64%). *R*_f = 0.18 (MeOH/DCM = 1:9); [α]_D²⁰ + 16.29 (*c* = 1 in MeOH); ¹H NMR (400 MHz, CD₃OD): δ = 4.81 (d, *J* = 1.5, 1H, H1), 3.79–3.87 (m, 3H), 3.56–3.74 (m, 15H), 3.48–3.56 (m, 6H), 3.35 (t, *J* = 5.6 Hz, 2H, -NHCH₂-), 3.26–3.32 (m, 4H, -NHCH₂- overlapped with CD₃OD), 2.38 (t, *J* = 7.4 Hz, 2H, -CH₂S-), 2.18 (t, *J* = 7.9 Hz, 2H, -(C=O)CH₂-), 1.53–1.65 (m, 4H, -CH₂-), 1.26–1.44 ppm (m, 12H, -CH₂-); ¹³C NMR (100 MHz, CD₃OD): δ = 176.7, 161.1, 101.7, 74.6, 72.5, 72.1, 71.6, 71.4, 71.3 (×3), 71.3, 71.2, 70.5, 68.6, 67.6, 62.9, 41.3, 41.2, 40.5, 36.8, 35.2, 30.6, 30.5, 30.4, 30.2, 30.2, 29.4, 27.0, 25.0 ppm; HRMS (ESI): *m/z* calcd for C₃₀H₅₈N₃O₁₂S [M-H]⁻: 684.3741; found: 684.3704.

Synthesis of compound 7

The fully protected thioacetate **22** was prepared using the procedures described in the synthesis of compound **21**, starting with **16** (500 mg, 0.99 mmol) and linker **13** (660.0 mg, 1.20 mmol). Purification by silica gel column chromatography afforded **22** (712 mg, 0.80 mmol, 80% over two steps). *R*_f = 0.37 (MeOH/DCM = 1:15); [α]_D²⁰ = +10.07 (*c* = 1.0 in MeOH); ¹H NMR (400 MHz, CD₃OD): δ = 5.20 (dd, *J* = 10.0, 10.0 Hz, 1H, H3), 4.97 (dd, *J* = 10.0, 10.0 Hz, 1H, H4), 4.70 (d, *J* = 8.4 Hz, 1H, H1), 4.27 (dd, *J* = 4.7, 12.4 Hz, 1H, H6a), 4.27 (dd, *J* = 2.4, 12.4 Hz, 1H, H6b), 3.92 (ddd, *J* = 4.2, 4.2, 11.1 Hz, 1H, -OCH₂-), 3.85 (dd, *J* = 8.4, 10.0 Hz, 1H, H2), 3.79 (ddd, *J* = 2.4,

4.7, 10.0 Hz, 1H, H5), 3.68–3.75 (m, 1H, -OCH₂-), 3.57–3.67 (m, 10H, -OCH₂-), 3.47–3.57 (m, 6H, -OCH₂-), 3.35 (t, *J* = 5.6 Hz, 2H, -NHCH₂-), 3.26–3.32 (m, 4H, -NHCH₂- overlapped with CD₃OD), 2.85 (t, *J* = 7.3 Hz, 2H, -CH₂S-), 2.29 (s, 3H, -(C=O)CH₃), 2.18 (t, *J* = 7.5 Hz, 2H, -(C=O)CH₂-), 2.04 (s, 3H, -(C=O)CH₃), 2.00 (s, 3H, -(C=O)CH₃), 1.97 (s, 3H, -(C=O)CH₃), 1.90 (s, 3H, -(C=O)CH₃), 1.49–1.65 (m, 4H, -CH₂-), 1.24–1.42 ppm (m, 12H, -CH₂-); ¹³C NMR (100 MHz, CDCl₃): δ = 195.9, 173.6, 170.7, 170.5, 169.2, 158.6, 101.0, 72.9, 71.4, 70.6, 70.5, 70.4, 70.3, 70.1, 69.9 (×2), 69.7, 68.6 (×2), 62.0, 53.9, 39.8, 39.6, 39.0, 36.3, 30.4, 29.2, 29.2 (×3), 29.0, 28.9, 28.8, 28.5, 25.5, 22.8, 20.5 (×2), 20.4 ppm; HRMS (ESI): *m/z* calcd for C₄₀H₇₀N₄O₁₆SNa [M+Na]⁺: 917.4405; found: 917.4407. Compound **7** was prepared using the procedures described above, starting with **22** (710 mg, 0.79 mmol). Purification by silica gel column chromatography yielded **7** (334 mg, 0.46 mmol, 58%). *R*_f = 0.42 (MeOH/DCM = 1:5); [α]_D²⁰ = +11.72 (*c* = 1.0 in MeOH); ¹H NMR (400 MHz, CD₃OD): δ = 4.45 (d, *J* = 8.3, 1H, H1), 3.94 (ddd, *J* = 3.8, 3.8, 11.2 Hz, 1H, -OCH₂-), 3.86 (dd, *J* = 2.1, 12.1 Hz, 1H, H6a), 3.56–3.73 (m, 14H, H2, H3, H6b, -OCH₂-), 3.42 (dd, *J* = 8.2, 10.2 Hz, 1H, H4), 3.22–3.37 (m, 7H, H5, -NHCH₂- overlapped with CD₃OD), 2.47 (t, *J* = 7.3 Hz, 2H, -CH₂S-), 2.17 (t, *J* = 7.7 Hz, 2H, -(C=O)CH₂-), 1.97 (s, 3H, -(C=O)CH₃), 1.52–1.64 (m, 4H, -CH₂-), 1.25–1.44 ppm (m, 12H, -CH₂-); ¹³C NMR (100 MHz, CD₃OD): δ = 176.2, 173.6, 160.9, 102.7, 77.9, 76.0, 72.0, 71.4 (×3), 71.4, 71.2 (×2), 71.2, 70.5, 69.8, 62.7, 57.1, 40.8 (×2), 40.2, 37.0, 35.1, 30.5, 30.5, 30.3, 30.2, 30.1, 29.3, 26.9, 25.1, 24.9, 23.1 ppm; HRMS (ESI): *m/z* calcd for C₃₂H₆₂N₄O₁₂SNa [M+Na]⁺: 749.3983; found: 749.3958.

Synthesis of compound 8

The fully protected thiolated fucoside **23** was prepared using the procedures described in the synthesis of compound **21**, starting with **17** (500.0 mg, 0.99 mmol) and linker **13** (683 mg, 1.23 mmol). Purification by silica gel column chromatography produced **23** (697 mg, 0.83 mmol, 74% over 2 steps). *R*_f = 0.42 (MeOH/DCM = 1:20); [α]_D²⁰ = +56.38 (*c* = 1.0 in MeOH); ¹H NMR (400 MHz, CD₃OD): δ = 5.33 (dd, *J* = 3.4, 10.9 Hz, 1H, H3), 5.26 (br d, *J* = 3.4 Hz, 1H, H4), 5.07 (d, *J* = 3.6 Hz, 1H, H1), 5.03 (dd, *J* = 3.6, 10.9 Hz, 1H, H2), 4.27 (br q, *J* = 6.5 Hz, 1H, H5), 3.76–3.84 (m, 1H, -OCH₂-), 3.57–3.72 (m, 11H, -OCH₂-), 3.45–3.56 (m, 6H, -OCH₂-), 3.34 (t, *J* = 5.4 Hz, 2H, -NHCH₂-), 3.25–3.31 (m, 4H, -NHCH₂- overlapped with CD₃OD), 2.84 (t, *J* = 7.2 Hz, 2H, -CH₂S-), 2.28 (s, 3H, -(C=O)CH₃), 2.17 (t, *J* = 7.6 Hz, 2H, -(C=O)CH₂-), 2.13 (s, 3H, -(C=O)CH₃), 2.04 (s, 3H, -(C=O)CH₃), 1.94 (s, 3H, -(C=O)CH₃), 1.39–1.55 (m, 4H, -CH₂-), 1.16–1.32 (m, 12H, -CH₂-), 1.02 ppm (d, *J* = 6.5 Hz, 3H, -CH₃); ¹³C NMR (100 MHz, CD₃OD): δ = 197.2, 176.2, 176.1, 172.1, 171.8, 171.5, 160.8, 97.4, 72.4, 71.6, 71.5, 71.5, 71.3 (×3), 71.2, 70.5, 69.3 (×2), 68.4, 65.5, 40.9, 40.8, 40.2, 37.0, 30.7, 30.6, 30.4 (×4), 30.3, 30.2, 30.1, 29.8, 29.7, 26.9, 20.7, 20.7, 20.5, 16.2 ppm; HRMS (ESI): *m/z* calcd for C₃₈H₆₇N₃O₁₅SNa [M+Na]⁺: 860.4191; found: 860.4151. Compound **8** was prepared using the procedure described for **6**, starting with **23** (340 mg, 0.41 mmol). Purification by flash silica gel column chromatography afforded thiolated fucoside **8** (160.0 mg, 0.24 mmol, 59%). *R*_f = 0.55 (MeOH/DCM = 1:9). [α]_D²⁰ = 51.23 (*c* = 1.0 in MeOH); ¹H NMR (400 MHz, CD₃OD): δ = 4.85 (d, *J* = 3.1, 1H, H1), 4.04 (br q, *J* = 6.6 Hz, 1H, H5), 3.84 (ddd, *J* = 4.0, 4.0, 10.5 Hz, 1H, -OCH₂-), 3.62–3.80 (m, 14H), 3.52–3.61 (m, 6H), 3.39 (t, *J* = 5.4 Hz, 2H, -NHCH₂-), 3.34 (t, *J* = 5.3 Hz, 4H, -NHCH₂- overlapped with CD₃OD), 2.52 (t, *J* = 7.1 Hz, 2H, -CH₂S-), 2.08 (t, *J* = 7.7 Hz, 2H, -(C=O)CH₂-), 1.56–1.76 (m, 4H, -CH₂-), 1.29–1.51 (m, 12H, -CH₂-), 1.25 ppm (d, *J* = 6.6 Hz, 3H, -CH₃); ¹³C NMR (100 MHz, CD₃OD): δ = 176.3, 161.0, 100.6, 73.5, 71.7, 71.6, 71.5, 71.5, 71.3, 71.2 (×3), 70.6, 70.0, 68.2, 67.6, 40.9, 40.8, 40.2, 37.0, 35.2, 30.6, 30.5, 30.4, 30.2,

30.2, 29.4, 27.0, 25.0, 16.7 ppm; HRMS (ESI): m/z calcd for $C_{30}H_{59}N_3O_{11}SNa$ [$M+Na$] $^+$: 692.3768; found: 692.3795.

Synthesis of compound 10

The sialyllactoside **24** was prepared according to the procedure described for **6**, starting with **18** (100 mg, 0.13 mmol) and linker **13** (90.0 mg, 0.16 mmol), with the exception that hydrogenation was performed in the absence of AcOH. Purification by size exclusion column chromatography on Bio-Gel P-2 afforded sialyllactoside **24** (108.0 mg, 0.09 mmol, 74% over two steps). $R_f=0.29$ (EtOAc/MeOH/H₂O/AcOH=3/2.5/0.5/0.5); $[\alpha]_D^{29}=-7.74$ ($c=2.4$ in MeOH); 1H NMR (400 MHz, D₂O): $\delta=4.41$ (d, $J=8.0$, 1H, Gal-H1), 4.33 (d, $J=7.8$, 1H, Glc-H1), 3.92–4.02 (m, 1H, -OCH₂-), 3.39–3.91 (m, 32H), 3.18–3.32 (m, 7H, -NHCH₂-, Sia-H5), 2.76 (t, $J=7.3$, 2H, -CH₂S-), 2.61 (dd, $J=4.5$, 12.2, 1H, Sia-H3a), 2.25 (s, 3H, -(C=O)CH₃), 2.14 (t, $J=7.3$, 2H, -(C=O)CH₂-), 1.93 (s, 3H, -(C=O)CH₃), 1.64 (dd, $J=12.2$, 12.2, 1H, Sia-H3b), 1.41–1.53 (m, 4H, -CH₂-), 1.10–1.30 ppm (m, 12H, -CH₂-); ^{13}C NMR (100 MHz, D₂O plus one drop CD₃OD): $\delta=200.5$, 177.2, 175.8, 174.3, 161.2, 104.2, 103.0, 101.2, 80.6, 75.6, 75.6, 74.6, 73.7, 73.5, 73.3, 72.7, 71.8, 70.9, 70.8, 70.7, 70.6, 70.5, 70.4, 70.0, 69.6, 69.5, 69.3, 69.3, 64.4, 63.6, 61.2, 60.3, 52.8, 41.0, 40.4 (×2), 39.9, 36.8, 31.2, 30.1 (×2), 30.0 (×2), 29.9, 29.8, 29.7, 29.4, 26.6, 23.0 ppm; HRMS (ESI): m/z calcd for $C_{49}H_{87}N_4O_{26}S$ [$M-H$] $^-$: 1179.5329; found: 1179.5316. Compound **24** (85 mg, 0.07 mmol) was dissolved in anhydrous MeOH (5.0 mL) and NaOMe (4.0 mg, 0.07 mmol). After stirring at room temperature for 30 min, the solution was neutralized with 1 M aqueous HCl and concentrated in vacuo. Purification by size exclusion column chromatography with deionized H₂O on Bio-Gel P-2 furnished thiolated sialyllactoside **10** (72 mg, 0.06 mmol, 88%). $R_f=0.24$ (EtOAc/MeOH/H₂O/AcOH=3/2.5/0.5/0.5); $[\alpha]_D^{29}=-6.84$ ($c=0.5$ in H₂O); 1H NMR (400 MHz, D₂O): $\delta=4.38$ (d, $J=7.7$, 1H, Gal-H1), 4.29 (d, $J=7.7$, 1H, Glc-H1), 3.88–3.99 (m, 1H, -OCH₂-), 3.31–3.88 (m, 35H), 3.11–3.30 (m, 7H, -NHCH₂-, Sia-H5), 2.57 (dd, $J=4.1$, 12.2, 1H, Sia-H3a), 2.40 (t, $J=7.0$, 2H, -CH₂S-), 2.11 (t, $J=7.0$, 2H, -(C=O)CH₂-), 1.89 (s, 3H, -(C=O)CH₃), 1.60 (dd, $J=12.2$, 12.2, 1H, Sia-H3b), 1.38–1.53 (m, 4H, -CH₂-), 1.06–1.33 ppm (m, 12H, -CH₂-); ^{13}C NMR (100 MHz, D₂O plus one drop CD₃OD): $\delta=178.1$, 175.9, 174.4, 161.3, 104.2, 103.0, 101.3, 80.6, 75.6, 75.6, 74.7, 73.7, 73.5, 73.3, 72.8, 71.8, 70.8 (×2), 70.7, 70.6, 70.5, 70.5, 70.4, 69.9, 69.7, 69.5, 69.3 (×2), 64.5, 63.6, 61.2, 52.8, 41.1, 40.4 (×2), 39.9, 36.7, 34.1, 29.7 (×2), 29.4, 29.2, 29.2, 28.6, 26.4, 24.8, 23.0 ppm; HRMS (ESI): m/z calcd for $C_{47}H_{85}N_4O_{25}S$ [$M-H$] $^-$: 1137.5224; found: 1137.5216.

Synthesis of compound 11

Palladium on carbon (Pd/C; 50 mg; 10% Pd content) was suspended in a solution of **19** (220 mg, 0.33 mmol) in MeOH (15 mL). The flask was purged with H₂, and a hydrogen balloon was attached. After stirring for 12 h at ambient temperature, the solution was filtered through a pad of Celite. The Celite bed was washed with MeOH, and the combined filtrates were concentrated under reduced pressure to provide the amine. Triethylamine (0.138 μ L, 0.99 mmol) and linker **13** (220.0 mg, 0.4 mmol) were added to a cold solution (-20 °C) of amine in a mixture of methanol and dichloromethane (15.0 mL, 1:1). The resulting mixture was warmed slowly to room temperature and stirred for 2 h until the starting material disappeared completely (determined by TLC). Following removal of volatiles in vacuo, the crude thioacetate (**25**) was redissolved in 1 M aqueous NaOH solution (20.0 mL). After stirring at room temperature for 30 min, the solution was neutralized with 1 M aqueous HCl and concentrated in vacuo. Purification by size exclusion chromatography on BioGel P-2 gel furnished thiolated P^K

trisaccharide derivative **11** (199 mg, 0.20 mmol, 60% over three steps). $R_f=0.45$ (EtOAc/MeOH/H₂O/AcOH=3/2.5/0.5/0.5); $[\alpha]_D^{29}=+30.11$ ($c=1.0$ in H₂O); 1H NMR (600 MHz, D₂O plus one drop CD₃OD): $\delta=4.87$ (d, $J=3.6$ Hz, α -Gal-H1), 4.40 (d, $J=7.7$ Hz, 1H), 4.37 (d, $J=7.9$ Hz, 1H), 4.24 (br t, $J=6.3$ Hz, 1H, α -Gal-H5), 3.97 (ddd, $J=4.2$, 4.2, 11.3 Hz, 1H), 3.95 (br d, $J=3.1$ Hz), 3.92 (dd, $J=1.0$, 3.0 Hz), 3.88 (dd, $J=2.1$, 12.3 Hz), 3.84 (dd, $J=2.1$, 12.3 Hz), 3.42–3.81 (m, 29H), 3.30 (t, $J=5.4$ Hz, 2H, -NHCH₂-), 3.21–3.26 (m, 5H, -NHCH₂-, Glc-H2), 2.62 & 2.44 (t, 2H, $J=7.2$ & 7.1 Hz, -CH₂S- from disulfide dimer & monomer, respectively), 2.15 (t, $J=7.4$ Hz, 2H, -(C=O)CH₂-), 1.46–1.55 (m, 4H, -CH₂-), 1.26–1.34 (m, 2H, -CH₂-), 1.15–1.26 ppm (m, 10H, -CH₂-); ^{13}C NMR (100 MHz, D₂O plus one drop CD₃OD): $\delta=176.4$, 161.0, 104.2, 103.1, 101.3, 79.8, 78.4, 76.3, 76.3, 75.7, 75.3, 73.9, 73.2, 71.9, 71.8, 70.9, 70.8, 70.7, 70.6 (×2), 70.6, 70.4, 70.1, 70.1, 70.0, 69.5, 61.6, 61.3, 61.1, 40.4 (×2), 39.8, 36.8, 34.7, 30.4 (×2), 30.2, 29.9 (×2), 29.2, 26.6, 25.2 ppm; HRMS (ESI): m/z calcd for $C_{42}H_{79}N_3O_{22}SNa$ [$M+Na$] $^+$: 1032.4774; found: 1032.4840.

Methods

Preparation of citrate-protected AuNPs (15 nm diameter)

All glassware used in the following reaction was cleaned with a freshly prepared Piranha solution (3 parts 18 M H₂SO₄, 1 part 30% H₂O₂) and then rinsed thoroughly with deionized water prior to use (**Caution!** Wear suitable protective apparel when handling highly corrosive acids). Spherical citrate-stabilized AuNPs were prepared through the Turkevich procedure.^[57] Briefly, 10 mL of 1% trisodium citrate (100 mg, 0.340 mmol) was added directly to a nitrogen-deaerated deionized water (200 mL) solution of HAuCl₄·3H₂O (44.5 mg, 0.113 mmol) under vigorous stirring at reflux. The solution was heated at reflux for an additional 15 min, and the solution became purple, and finally turned dark red. The resulting solution was cooled gradually to room temperature, and the UV/Vis absorption spectrum indicated an SPR band centered at 520 ± 1 nm (see the Supporting Information, Figure S1). The average size of the metal core of these glyco-AuNPs was 15.2 ± 1.5 nm, as determined by TEM (Figure S1). The citrate-protected AuNPs (pH 5.87) could be stored at 4 °C for several months or until use in the ligand-exchange reaction with thiolated carbohydrates (see below).

General procedures for the ligand-exchange reaction and the purification of glyco-AuNPs

Glyco-AuNPs were synthesized in a one-step ligand-exchange reaction between citrate-stabilized AuNPs and thiolated glycans (**1–4** and **6–11**, respectively) following established procedures.^[25,26] Briefly, reduced thiolated glycans **1–4** (0.004 mmol) were added to a solution of nitrogen-deaerated citrate-protected AuNPs (40 mL). The pH of the solution was adjusted to 11 with a 0.1 M NaOH aqueous solution. The resulting mixture was stirred at room temperature for 48 h. The glyco-AuNPs were purified by centrifugation at 8000 ×g, and the gold sol obtained was redispersed in either NaCl-free buffer (Tris buffer, 10 mM, pH 7.4) or NaCl-containing phosphate-buffered saline (PBS, pH 7.4). The centrifugation and redispersion processes were repeated three times to remove any excess thiolated glycans or other reactants. UV/Vis absorption spectra were then acquired to examine NP aggregation to ensure that the NPs did not aggregate during modification.

Preparation of mixed monolayer-protected glyco-AuNPs (5-AuNP to 11-AuNP)

For the preparation of 5-AuNP to 11-AuNP, a mixed thiol solution was prepared from the corresponding thiolated glycans (70 mol%) and linker **12** (30 mol%). The ligand-exchange reaction of the AuNPs with mixed thiols followed the general functionalization method described above, with the exception that the pure thiol was replaced with the mixed thiol solution for the treatment of the citrate-stabilized AuNPs. The remainder of the coupling was performed following the same method described in detail above. The concentration of the glyco-AuNP solution, approximately 20 nM, was determined by measuring the SPR absorption and using a reported^[58] extinction coefficient ($3.64 \times 10^8 \text{ M}^{-1} \text{ cm}^{-1}$) to provide 5-AuNP, 6-AuNP, 7-AuNP, 8-AuNP, 9-AuNP, 10-AuNP, and 11-AuNP. These glyco-AuNPs could be stored at 4 °C for several months until use.

Stability of glyco-AuNPs in NaCl-containing aqueous buffer

The effect of NaCl on the stability of AuNPs was studied by a colorimetric assay following a protocol described previously.^[26] Thiol-terminated lactose derivatives **1–4** (0.1 mM) were allowed to react with citrated-protected AuNPs (5 nm) for 48 h. The resulting lactose-functionalized AuNPs were divided (200 μL) into 96-well microtiter plates without purification. NaCl was added to the wells to obtain final concentrations of 0, 12.5, 25, 50, 100, 150, 300, and 600 mM. Following a 1 h incubation, the absorbance at 620 nm was recorded with an ELISA plate reader (SpectraMax M2^e, Molecular Devices).

Nonspecific protein adsorption on glyco-AuNPs

BSA was used to measure nonspecific protein adsorption on glyco-AuNPs. Glyconanoparticles (such as 5-AuNP, 3 nm, 1 mL) were incubated with varying concentrations of BSA (0, 0.02, 2, 200 μM) at room temperature for 8 h. The solution was monitored by UV/Vis spectrophotometry and a particle size analyzer.

Plate-based colorimetric detection of lectins by glyco-AuNPs

In regular 96-well microtiter plates, solutions of glyco-AuNPs (3 nm) in PBS buffer containing 0.005% Tween 20 (PBST, 200 μL) were incubated with cognate lectins (500 nM) at room temperature for 2 h. Following incubation, the change in absorbance from 450–750 nm was measured with an ELISA plate reader as described above.^[26]

Fabrication of the random-immobilized antibody slide

For the immobilization of antibodies on a glass slide, microarrays were generated using a AD1500 arrayer (contact mode) to print antibodies (6.7 μM in PBS buffer, pH 7.4) onto a NEXTERION Slide H with a contact time of 300 ms. The resulting slides were incubated at 4 °C overnight. Then, all of the remaining unreacted activated ester groups were capped by incubation with a capping reagent (see general information) at 25 °C for 1 h. After incubation, the glass slide was washed sequentially with PBST, PBS, and deionized H₂O for 5 min each and finally dried by centrifugation. The antibody slide was stored in the proper chamber at 4 °C prior to further use.

Fabrication of the oriented immobilized antibody slide

Nexterion H glass slides were treated with a 50 mM solution of **26** in PBS (pH 8.5) at room temperature for 24 h to derivatize the *N*-hydroxysuccinimide (NHS)-ester groups. The slides were washed with deionized water and then dried by centrifugation. The unreacted NHS-esters were deactivated by immersing the slide into a solution containing ethanolamine (25 mM) in borate buffer (100 mM, pH 9.2) at room temperature for 1 h. The slides were washed sequentially with phosphate-buffered saline (PBS, pH 7.4) and PBS containing 0.05% Tween 20 (PBST), rinsed with deionized water, and dried prior to use. Monoclonal capture antibodies (6.6 μM in PBS buffer, pH 7.4) were dispensed by using a robotic contact arrayer (AD1500 Arrayer, BioDot) fitted with Stealth Pins SMP3 (ArrayIt Corporation) onto **26**-functionalized glass slides. The printing process was performed at a relative humidity of 94%, and the temperature was maintained below 26 °C. The slide was allowed to react at 4 °C for 24 h; this was followed by rinsing with deionized H₂O to remove any unbound antibodies. The remaining BAs on the surface were then blocked with dextran (100 μM) containing 1% BSA in water at room temperature for 2 h to prevent nonspecific adhesion/interactions. Following a wash, the oriented-antibody immobilized microarray slides could be probed with cognate lectin and glyco-AuNPs either in a layer-by-layer format or in situ agglutination for detection with the naked eye (see below).

In situ lectin-induced AuNP agglutination on microarrays and naked-eye detection through silver enhancement

The oriented immobilized antibody slide was incubated with 100 μL of a solution containing a mixture of lectin and glyco-AuNPs (5 nm) for 2–8 h at room temperature. A 16-well incubation chamber (Whatman, Inc.) was used to divide the slide into 16 blocks (each with a 9 \times 9 mm format) to prevent cross-contamination when different samples were applied to neighboring blocks. After incubation, the unbound materials were removed by sequential washing with PBST, PBS, and deionized H₂O for 5 min each. Finally, the glass slide was dried by centrifugation, and the bound AuNPs were further visualized by silver enhancement for 14 min unless otherwise noted. In silver enhancement, the AuNPs act as the nucleation sites for metallic silver, enabling visual detection of the darkened, enlarged sites.

Acknowledgements

This work was supported financially by the National Tsing Hua University, Academia Sinica, and the Ministry of Science and Technology of Taiwan.

Keywords: antibodies • biosensors • boronic acid • nanoparticles • lectins

- [1] C. Fasting, C. A. Schalley, M. Weber, O. Seitz, S. Hecht, B. Kokschi, J. Drenth, C. Graf, E. W. Knapp, R. Haag, *Angew. Chem. Int. Ed.* **2012**, *51*, 10472–10498; *Angew. Chem.* **2012**, *124*, 10622–10650.
- [2] *Lectins*, 2nd ed. (Eds.: N. Sharon, H. Lis), Kluwer Academic, Dordrecht, **2003**.
- [3] W. I. Weis, K. Drickamer, *Annu. Rev. Biochem.* **1996**, *65*, 441–473.
- [4] J. Stevens, O. Blixt, L. Glaser, J. K. Taubenberger, P. Palese, J. C. Paulson, I. A. Wilson, *J. Mol. Biol.* **2006**, *355*, 1143–1155.
- [5] S. Fukuta, J. L. Magnani, E. M. Twiddy, R. K. Holmes, V. Ginsburg, *Infect. Immun.* **1988**, *56*, 1748–1753.

- [6] T. B. Geijtenbeek, D. S. Kwon, R. Torensma, S. J. van Vliet, G. C. van Duijnhoven, J. Middel, I. L. Cornelissen, H. S. Nottet, V. N. KewalRamani, D. R. Littman, C. G. Figdor, Y. van Kooyk, *Cell* **2000**, *100*, 587–597.
- [7] L. L. Kiessling, R. A. Splain, *Annu. Rev. Biochem.* **2010**, *79*, 619–653.
- [8] J. E. Turnbull, R. A. Field, *Nat. Chem. Biol.* **2007**, *3*, 74–77.
- [9] D. A. Giljohann, C. A. Mirkin, *Nature* **2009**, *462*, 461–464.
- [10] K. Saha, S. S. Agasti, C. Kim, X. Li, V. M. Rotello, *Chem. Rev.* **2012**, *112*, 2739–2779.
- [11] M. Marradi, F. Chiodo, I. Garcia, S. Penadés, *Chem. Soc. Rev.* **2013**, *42*, 4728–4745.
- [12] J. M. de la Fuente, A. G. Barrientos, T. C. Rojas, J. Rojo, J. Canada, A. Fernandez, S. Penadés, *Angew. Chem. Int. Ed.* **2001**, *40*, 2257–2261; *Angew. Chem.* **2001**, *113*, 2317–2321.
- [13] C.-C. Lin, Y.-C. Yeh, C.-Y. Yang, C.-L. Chen, G.-F. Chen, C.-C. Chen, Y.-C. Wu, *J. Am. Chem. Soc.* **2002**, *124*, 3508–3509.
- [14] A. G. Barrientos, J. M. de La Fuente, T. C. Rojas, A. Fernandez, S. Penadés, *Chem. Eur. J.* **2003**, *9*, 1909–1921.
- [15] C. L. Schofield, A. H. Haines, R. A. Field, D. A. Russell, *Langmuir* **2006**, *22*, 6707–6711.
- [16] S. Takae, Y. Akiyama, H. Otsuka, T. Nakamura, Y. Nagasaki, K. Kataoka, *Biomacromolecules* **2005**, *6*, 818–824.
- [17] C. L. Schofield, B. Mukhopadhyay, S. M. Hardy, M. McDonnell, R. A. Field, D. A. Russell, *Analyst* **2008**, *133*, 626–634.
- [18] A. K. Adak, H.-J. Lin, C.-C. Lin, *Org. Biomol. Chem.* **2014**, *12*, 5563–5573.
- [19] C.-C. Lin, Y.-C. Yeh, C.-Y. Yang, G.-F. Chen, Y.-C. Che, Y.-C. Wu, C.-C. Chen, *Chem. Commun.* **2002**, 2920–2921.
- [20] Y. Zhang, S. Luo, Y. Tang, L. Yu, K.-Y. Hou, J.-P. Cheng, X. Zheng, P. G. Wang, *Anal. Chem.* **2006**, *78*, 2001–2008.
- [21] J. M. de La Fuente, P. Eaton, A. G. Barrientos, M. Menendez, S. Penadés, *J. Am. Chem. Soc.* **2005**, *127*, 6192–6197.
- [22] K. El-Boubbou, D. C. Zhu, C. Vasileiou, B. Borhan, D. Prosperi, W. Li, X. Huang, *J. Am. Chem. Soc.* **2010**, *132*, 4490–4499.
- [23] X. Wang, O. Ramström, M. Yan, *Anal. Chem.* **2010**, *82*, 9082–9089.
- [24] X. Wang, O. Ramström, M. Yan, *Analyst* **2011**, *136*, 4174–4178.
- [25] Y.-Y. Chien, M.-D. Jan, A. K. Adak, H.-C. Tzeng, Y.-P. Lin, Y.-J. Chen, K.-T. Wang, C.-T. Chen, C.-C. Lin, *ChemBioChem* **2008**, *9*, 1100–1109.
- [26] C.-C. Yu, L.-D. Huang, D. H. Kwan, W. W. Wakarchuk, S. G. Withers, C.-C. Lin, *Chem. Commun.* **2013**, *49*, 10166–10168.
- [27] A. J. Reynolds, A. H. Haines, D. A. Russell, *Langmuir* **2006**, *22*, 1156–1163.
- [28] E. Mabon, T. Astrup, M. Barboiu, *Chem. Commun.* **2010**, *46*, 5491–5493.
- [29] E. Ostuni, R. G. Chapman, M. N. Liang, G. Pier, D. E. Ingber, G. M. Whitesides, *Langmuir* **2001**, *17*, 6336–6343.
- [30] T.-H. Yang, L.-D. Huang, Y.-W. Harm, C.-C. Lin, J.-K. Chang, C.-I. Wu, J.-M. Wu, *Small* **2013**, *9*, 3169–3182.
- [31] J. J. Storhoff, A. A. Lazarides, R. C. Mucic, C. A. Mirkin, R. L. Letsinger, G. C. Schatz, *J. Am. Chem. Soc.* **2000**, *122*, 4640–4650.
- [32] D. C. Hone, A. H. Haines, D. A. Russell, *Langmuir* **2003**, *19*, 7141–7144.
- [33] D. J. Vanderah, J. Arsenaault, H. La, R. S. Gates, V. Silin, C. W. Meuse, *Langmuir* **2003**, *19*, 3752–3756.
- [34] M. Zheng, F. Davidson, X. Huang, *J. Am. Chem. Soc.* **2003**, *125*, 7790–7791.
- [35] S. K. Podder, A. Suroliya, B. K. Bachhawat, *Eur. J. Biochem.* **1974**, *44*, 151–160.
- [36] M. Huet, *Eur. J. Biochem.* **1975**, *59*, 627–633.
- [37] G. Bains, R. T. Lee, Y. C. Lee, E. Freire, *Biochemistry* **1992**, *31*, 12624–12628.
- [38] K. Matsumura, K. Higashida, H. Ishida, Y. Hata, K. Yamamoto, M. Shigeta, Y. M. Horikawa, X. Wang, E. Miyoshi, J. Gu, N. Taniguchi, *J. Biol. Chem.* **2007**, *282*, 15700–15708.
- [39] W.-C. Wang, R. D. Cummings, *J. Biol. Chem.* **1988**, *263*, 4576–4585.
- [40] N. Shibuya, I. J. Goldstein, W. F. Broekaert, M. Lubaki, B. Peters, *J. Biol. Chem.* **1987**, *262*, 1596–1601.
- [41] N. Gilboa-Garber, D. Sudakevitz, M. Sheffi, R. Sela, C. Levene, *Glycoconjugate J.* **1994**, *11*, 414–417.
- [42] X. Song, H. Yu, X. Chen, Y. Lasanajak, M. M. Tappert, G. M. Air, V. K. Tiwari, H. Cao, H. A. Chokhawala, H. Zheng, R. D. Cumming, D. F. Smith, *J. Biol. Chem.* **2011**, *286*, 31610–31622.
- [43] J. C. Manimala, T. A. Roach, Z. T. Li, J. C. Gildersleeve, *Angew. Chem. Int. Ed.* **2006**, *45*, 3607–3610; *Angew. Chem.* **2006**, *118*, 3689–3692.
- [44] B. P. Peters, S. Ebisu, I. J. Goldstein, M. Flashner, *Biochemistry* **1979**, *18*, 5505–5511.
- [45] E. Song, J. Li, H. Wei, Y. Song, *Anal. Methods* **2012**, *4*, 1199–1201.
- [46] M.-L. Chen, A. K. Adak, N.-C. Yeh, W.-B. Yang, Y.-J. Chuang, C.-H. Wong, K.-C. Hwang, J.-R. Hwu, S.-L. Hsieh, C.-C. Lin, *Angew. Chem. Int. Ed.* **2008**, *47*, 8627–8630; *Angew. Chem.* **2008**, *120*, 8755–8758.
- [47] P.-C. Lin, S.-H. Chen, M.-L. Chen, A. K. Adak, Y.-J. Chen, C.-C. Lin, *Anal. Chem.* **2009**, *81*, 8774–8782.
- [48] A. K. Adak, B.-Y. Li, L.-D. Huang, T.-W. Lin, T.-C. Chang, K.-C. Hwang, C.-C. Lin, *ACS Appl. Mater. Interfaces* **2014**, *6*, 10452–10460.
- [49] P.-C. Lin, P.-H. Chou, S.-H. Chen, H.-K. Liao, K.-Y. Wang, Y.-J. Chen, C.-C. Lin, *Small* **2006**, *2*, 485–489.
- [50] J.-A. Ho, W.-L. Hsu, W.-C. Liao, J.-K. Chiu, M.-L. Chen, H.-C. Chang, C.-C. Lin, *Biosens. Bioelectron.* **2010**, *26*, 1021–1027.
- [51] V. Wittmann, R. J. Pieters, *Chem. Soc. Rev.* **2013**, *42*, 4492–4502.
- [52] H. Kato, H. Uzawa, T. Nagatsuka, S. Kondo, K. Sato, I. Ohsawa, M. Kanamori-Kataoka, Y. Takei, S. Ota, M. Furuno, H. Dohi, Y. Nishida, Y. Seto, *Carbohydr. Res.* **2011**, *346*, 1820–1826.
- [53] L. Deng, O. Norberg, S. Uppalapati, M. Yan, O. Ramstrom, *Org. Biomol. Chem.* **2011**, *9*, 3188–3198.
- [54] F. Sallas, S.-I. Nishimura, *J. Chem. Soc. Perkin Trans. 1* **2000**, 2091–2103.
- [55] F. Morvan, A. Meyer, A. Jochum, C. Sabin, Y. Chevolut, A. Imbert, J.-P. Praly, J.-J. Vasseur, E. Souteyrand, S. Vidal, *Bioconjugate Chem.* **2007**, *18*, 1637–1643.
- [56] S.-P. Li, W.-C. Hsiao, C.-C. Yu, W.-T. Chien, H.-J. Lin, L.-D. Huang, C.-H. Lin, W.-L. Wu, S.-H. Wu, C.-C. Lin, *Adv. Synth. Catal.* **2014**, *356*, 3199–3213.
- [57] B. V. Enüstün, J. Turkevich, *J. Am. Chem. Soc.* **1963**, *85*, 3317–3324.
- [58] W. Lian, D. Wu, D. V. Lim, S. Jin, *Anal. Biochem.* **2010**, *401*, 271–279.

Received: October 21, 2014

Published online on January 8, 2015